CORE
Metadata, citation and similar papers at core.ac.uk
Provided by Digital.CSIC

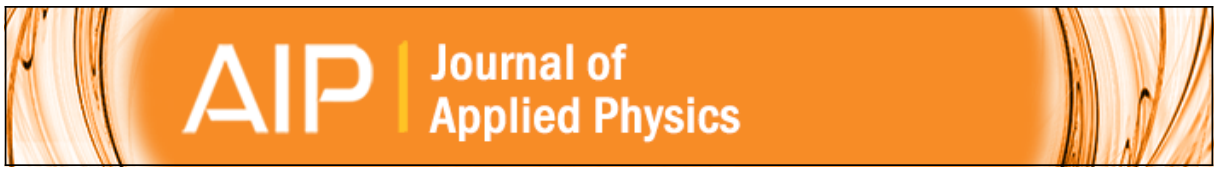

Laser ablation of ceramic Al2O3 at 193 nm and 248 nm: The importance of single-photon ionization processes

R. J. Peláez, C. N. Afonso, M. Bator, and T. Lippert

Citation: Journal of Applied Physics **113**, 223301 (2013); doi: 10.1063/1.4809639
View online: http://dx.doi.org/10.1063/1.4809639
View Table of Contents: http://scitation.aip.org/content/aip/journal/jap/113/22?ver=pdfcov
Published by the AIP Publishing

Articles you may be interested in

Photodissociation of the propargyl and propynyl (C 3 D 3) radicals at 248 and 193 nm
J. Chem. Phys. **130**, 044310 (2009); 10.1063/1.3067705

Photofragment translation spectroscopy of Cl N 3 at 248 nm: Determination of the primary and secondary dissociation pathways
J. Chem. Phys. **123**, 104305 (2005); 10.1063/1.1948381

Selective ablation of AlN ceramic using femtosecond, nanosecond, and microsecond pulsed laser
J. Appl. Phys. **89**, 2943 (2001); 10.1063/1.1342805

Competing dissociation between the S–Cl and S–S bonds in the photolysis of S 2 Cl 2 at 248 and 193 nm
J. Chem. Phys. **110**, 6812 (1999); 10.1063/1.478585

APL Photonics

Reuse of AIP Publishing content is subject to the terms at: https://publishing.aip.org/authors/rights-and-permissions. Download to IP: 161.111.22.69 On: Fri, 08 Jul 2016 09:42:42

Laser ablation of ceramic Al_2O_3 at 193 nm and 248 nm: The importance of single-photon ionization processes

R. J. Peláez,[1] C. N. Afonso,[1] M. Bator,[2] and T. Lippert[2]
[1]*Laser Processing Group, Instituto de Optica, CSIC, Serrano 121, Madrid 28006, Spain*
[2]*General Energy Research Department, Paul Scherrer Institut, CH-5232 Villigen PSI, Switzerland*

(Received 15 April 2013; accepted 21 May 2013; published online 10 June 2013)

The aim of this work is to demonstrate that single-photon photoionization processes make a significant difference in the expansion and temperature of the plasma produced by laser ablation of ceramic Al_2O_3 in vacuum as well as to show their consequences in the kinetic energy distribution of the species that eventually will impact on the film properties produced by pulsed laser deposition. This work compares results obtained by mass spectrometry and optical spectroscopy on the composition and features of the plasma produced by laser ablation at 193 nm and 248 nm, i.e., photon energies that are, respectively, above and below the ionization potential of Al, and for fluences between threshold for visible plasma and up to ≈2 times higher. The results show that the ionic composition and excitation of the plasma as well as the ion kinetic energies are much higher at 193 nm than at 248 nm and, in the latter case, the population of excited ions is even negligible. The comparison of Maxwell-Boltzmann temperature, electron temperatures, and densities of the plasmas produced with the two laser wavelengths suggests that the expansion of the plasma produced at 248 nm is dominated by a single population. Instead, the one produced at 193 nm is consistent with the existence of two populations of cold and hot species, the latter associated to Al^+ ions that travel at the forefront and produced by single photon ionization as well as Al neutrals and double ionized ions produced by electron-ion impact. The results also show that the most energetic Al neutrals in the plasma produced at the two studied wavelengths are in the ground state.
© *2013 AIP Publishing LLC*. [http://dx.doi.org/10.1063/1.4809639]

I. INTRODUCTION

Pulsed laser deposition (PLD) has proved to be an attractive technique for producing thin films of many materials that is particularly suited for producing oxide films. Generally, a gas background is required for producing good quality oxide films in order to achieve the appropriate stoichiometry. However, a gas background is well known to slow down the velocity of the species arriving at the substrate,[1] while special features or improved performance of films have been related to their high kinetic energy (KE),[2–6] particularly to ions having KE > 200 eV.[7] Discussion on the impact of species KE on film growth are generally based on mean KE values that are typically of tens of eV and vary little with fluence.[8,9] Instead, KE distributions are known to expand significantly over hundreds of eVs when the fluence is increased.[1,7–9]

Al_2O_3 is an interesting oxide, e.g., as a material for optical applications due to its high stability and refractive index that is higher than that of SiO_2.[2,10] There are some works relating the plasma and film properties reporting that the film structure depends on the mean KE of species[4] and that the film density and refractive index increase as fluence is increased or the processing gas pressure is decreased.[2,10] In addition, stoichiometric and good quality films can be grown in vacuum.[5,11]

Al_2O_3 is a simple oxide, whose cation is the one of the few metals that has an ionization potential (5.98 eV) smaller than one of the photon energies typically used in PLD (6.4 eV from excimer laser operating at 193 nm). In spite of the plasma produced by ablation of Al_2O_3 at 193 nm offers an excellent case for studying the importance of single-photon ionization processes, there are almost no reports in the literature using this wavelength. There are some early reports on the ionic content and kinetics of the plasma produced by ablation of single crystalline c-Al_2O_3 (sapphire) in vacuum using nanosecond pulses at 248 nm and fluences above the plasma formation threshold.[12,13] The aim of this study was an understanding of the mechanism of ablation and it concluded that there was evidence for its electronic rather than thermal nature. The works on laser ablation of ceramic Al_2O_3 targets also relate to single wavelengths of 248 nm,[3,14] 355 nm,[15] 532 nm,[11] or 1064 nm.[4] Only recently, the ion yield and KE distributions produced by ablation of a ceramic Al_2O_3 target at 193 nm have been reported showing that Al^+ represent >80% of the ions[16] and 20% of the ions had KE > 200 eV around the threshold for plasma formation.[17] These results were related to the existence of direct photoionization processes in the plasma. It was also shown that the kinetics of ions in the plasma produced by ablation of ceramic Al_2O_3 and Al at 193 nm is very similar.[17] An earlier work comparing the plasmas produced by ablating Al and Al_2O_3 targets at 248 nm has shown that the electron density associated with Al species is nearly two times higher for Al_2O_3 than in the case of Al.[14]

The plasma produced by laser ablation of Al has instead been widely studied using several approaches and reporting a broad range of plasma properties. Several laser

 © 2013 AIP Publishing LLC

Reuse of AIP Publishing content is subject to the terms at: https://publishing.aip.org/authors/rights-and-permissions. Download to IP: 161.111.22.69 On: Fri, 08 Jul 2016 09:42:42

wavelengths have been used: 193 nm,[8,17] 248 nm,[14,18–20] 308 nm,[21,22] 351 nm,[18] 355 nm,[23] 532 nm,[23,24] and 1064 nm.[25] It is generally reported that the ionization is higher for shorter wavelengths,[23] that saturation effects in ion yield at high fluences exist,[23] and that the KE distributions are generally well fitted with shifted Maxwell-Boltzmann distributions,[20,23,24] although there is one early work in which the velocity distribution of Al was reported as hyperthermal and not Maxwellian.[18] Comparing the KE distributions reported in the studies performing ablation of Al at different wavelengths, the ions produced upon 193 nm have the higher KE values[8,17] and this has been related to the photon energy being higher than the ionization potential of Al. Furthermore, an early work on ablation of Al in H_2 at both 193 nm and 248 nm highlighted the importance of photoionization processes in the plasma expansion for 193 nm ablation.[26]

The aim of this work is to compare for the first time the plasma ionic composition and features upon ablation of a ceramic Al_2O_3 target in vacuum at 193 nm and 248 nm under the same conditions and at fluences typically used for PLD. The ultimate aim is to identify clearly if single-photon photoionization processes make any significant difference in the plasma expansion and temperature as well as which are their consequences in the KE distribution (N(E)) of the species that eventually will have a direct impact on the film properties.

II. EXPERIMENTAL

An ArF excimer laser ($\lambda = 193$ nm, $\tau = 20$ ns, Lambda Physik LPX 300) and a KrF ($\lambda = 248$ nm, $\tau = 34$ ns, Lambda-Physik LPX200) were used for ablating a cylindrical ceramic Al_2O_3 target in vacuum ($<10^{-6}$ mbar). The laser beams were imaged on the target surface at 45° to spot areas of $\approx 0.9 \times 0.7$ mm^2 and $\approx 0.8 \times 0.8$ mm^2 leading to fluences up to 2 J/cm^2 and 4 J/cm^2 for the ArF and KrF laser beams, respectively.

Two main diagnostics tools were used to study the composition and dynamics of the plasma produced by laser ablation along its axis. The first one was an electrostatic quadrupole mass spectrometer (EQP-QMS Hiden) that was placed along the direction perpendicular to the impact point of the laser on the target. The species go first into an ionizer stage through a nozzle (diameter of 0.6 mm) located at 4 cm from the target. For charged species analysis, the ionizer is switched off and the species become deflected according to their mass to charge ratio. For neutral species analysis, the ionizer is switched on and a field is applied to the EQP extractor to reject all incoming charged species. The amount of species that are finally collected by the detector is thus affected by their ionization cross section. A quantitative comparison between the amount of charged and neutral species and among different neutral species is therefore not straightforward. The system allows measuring KE up to 100 eV and acquisitions were performed using a delay of 20 μs with respect to the signal of a photodiode collecting the laser output and an acquisition time of 400 μs. Since in an earlier work using the same experimental approach it was shown that the more relevant and faster species were monoatomic species,[16] we focus the present work to these species.

The second diagnostic tool was imaging emission spectroscopy. The plasma that expands along the direction perpendicular to the target surface is imaged onto the entrance slit of an Acton SP 500 spectrograph using two achromatic lenses and a periscope in order to align the expansion direction along the entrance slit of the spectrograph. The output of the spectrograph is a 1D-spatial and 1D-spectral image of the expanding plasma that is recorded with an ICCD 1024 MLDG-E/1 and an EEV 256 × 1024 (6 ph) sensor. Series of time-gated spatial-spectral images have been recorded using a gate width of 25 ns and a delay with respect to the laser pulse in the range 30–660 ns that was varied in steps of 70 ns. Each image consists of 10 accumulations covering a spectral interval of 15–20 nm that was varied in the range 250–800 nm and has been background-subtracted. More details on the experimental setup and data processing can be found elsewhere.[27,28]

III. RESULTS

Figures 1(a) and 1(b), respectively, show a comparison of the KE distributions of relevant positively charged ions

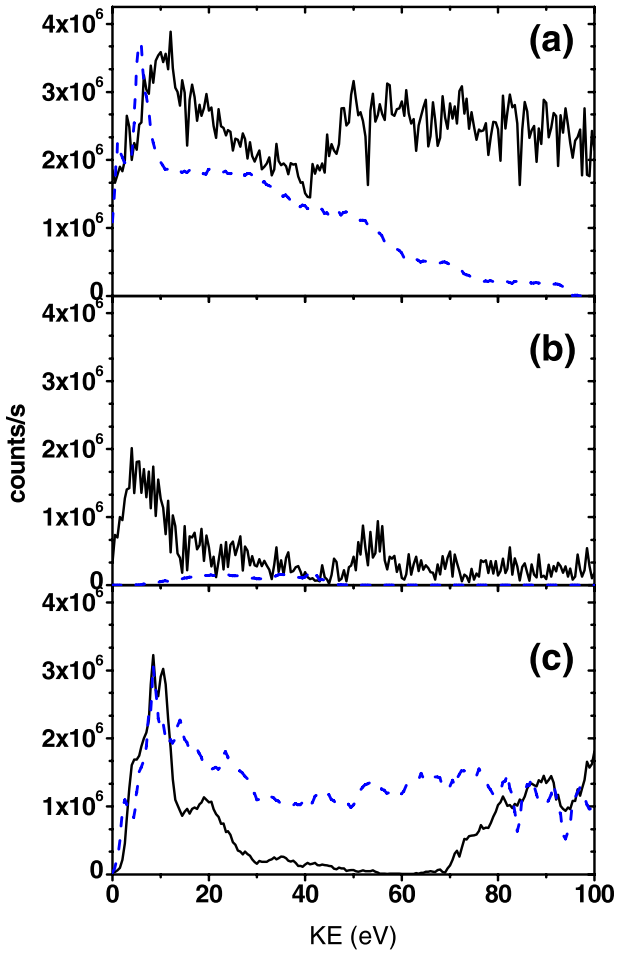

FIG. 1. KE distributions at $z = 4$ cm obtained by mass spectrometry of (a) Al^+, (b) O^+, and (c) Al upon ablation at 193 nm (full line) at 0.4 J/cm^2 ((a) and (b)) and 2 J/cm^2 (c), and 248 nm (dashed line) at 1.6 J/cm^2 ((a) and (b)) and 4 J/cm^2 (c).

Reuse of AIP Publishing content is subject to the terms at: https://publishing.aip.org/authors/rights-and-permissions. Download to IP: 161.111.22.69 On: Fri, 08 Jul 2016 09:42:42

(Al^+, O^+) obtained upon ablation using the two studied wavelengths. We have selected fluences close to the threshold for obtaining visible plasma for each wavelength. The most striking result is the almost constant KE of Al^+ species upon ablation at 193 nm. This result suggests that even at this very low fluence, there is a significant amount of these ions having KEs above 100 eV (Fig. 1(a)). Instead, the KE distribution of Al^+ upon ablation at 248 nm shows a maximum at low KEs that is followed by a long decrease leading to an almost negligible amount of ions with KE of 100 eV. As fluence is increased (not shown), the KE distribution at 193 nm remains constant while that at 248 nm becomes similar to that obtained at 193 m. For O^+ (Fig. 1(b)), most of the ions have KE < 20 eV when ablating at 193 nm, while their amount is comparatively negligible for ablation at 248 nm. As fluence is increased (not shown), the KE distribution shows that the amount of ions at all energies upon ablation at 193 nm increases and becomes significant for KE = 100 eV. For 248 nm ablation, this amount develops into a broad maximum that extends up to 30 eV (similar to that observed for the case of ablation at 193 nm at low fluences shown in Fig. 1(b)) to become negligible for KE > 40 eV.

Figure 1(c) shows the KE distributions of Al neutrals for the highest studied fluence upon ablation at the two studied wavelengths. For ablation at 248 nm, the distribution is almost flat with the exception of a maximum at low KEs (~10 eV). For ablation at 193 nm, a maximum is observed at approximately the same low KE. After this maximum, the distribution becomes almost negligible in the range 40–70 eV to increase for higher KEs. At both wavelengths, there is a similar significant amount of species with KE around 100 eV. While the described features apply to all fluences studied for the case of ablation at 248 nm, there is a significant change when the fluence is decreased for ablation at 193 nm. In this case, the maximum at high energies decreases until it becomes negligible with decreasing fluence. Instead, the maximum at low energies shows little changes with fluence.

The fluence dependence of the amount of studied species can be seen in Fig. 2 for Al^+ (Fig. 2(a)), Al (Fig. 2(b)) and O^+ (Fig. 2(c)) upon ablation with the two studied wavelengths. We have plotted the relative amount obtained by integrating the KE distributions (such as those plotted in Fig. 1) for each fluence and normalizing the result by the value obtained for the highest studied fluence in each case. Therefore, all curves should approach unity. For Al species, an approximately constant amount of Al^+ is observed when using 193 nm that is different to the increase from a threshold value up to saturation that occurs for fluences of ~2 J/cm^2 when using 248 nm. In contrast, the amount of Al is approximately constant for both wavelengths (Fig. 1(b)). In absolute terms (not shown), the amount of Al is approximately twice for 248 nm than for 193 nm ablation. Figure 1(c) shows that the KE energy distribution has two maxima with different evolution with fluence upon ablation at 193 nm. Since the second maxima starts at ~70 eV, the inset in Fig. 2(b) shows in absolute terms the amount of Al with KE above and below this value as a function of fluence. It can be seen that the amount of fast species increases while the amount of slow

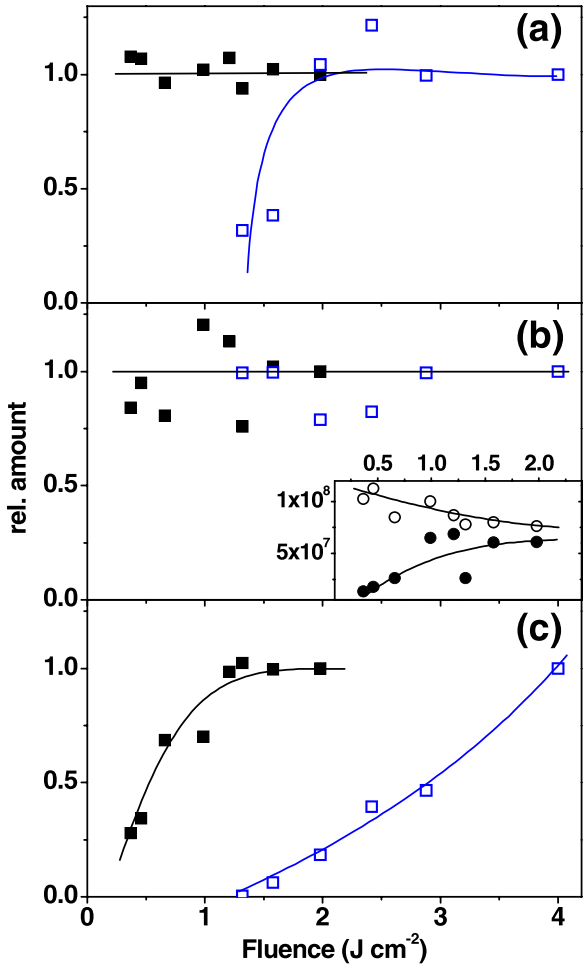

FIG. 2. Relative amount of (a) Al^+, (b) Al, and (c) O^+ species at $z = 4$ cm as a function of fluence upon ablation at (■) 193 nm and (□) 248 nm. The normalization factor is the value at the highest fluence studied in each case. The inset in (b) shows the absolute amount of Al species having (○) KE < 70 eV and (●) KE > 70 eV as a function of fluence. Lines are guidelines.

species decreases with increasing fluence. Finally, it is worth to mention that upon ablation at 248 nm, no Al^{++} was detected whereas for 193 nm ablation, the relative amount increases with fluence and shows no evidences of saturation in the studied fluence range as reported earlier.[16]

The amount of O^+ (Fig. 2(c)) follows the expected trend for both wavelengths, i.e., an increase with increasing fluence, and the O^+ produced at 193 nm nearly reaches saturation for fluences which are close to the threshold for observing O^+ at 248 nm. It is worth to mention here that in the context of Fig. 2, the saturation observed might be only apparent due to the fact that the KE distributions in Fig. 1 have the upper limit of 100 eV due to the mass spectrometer range of detection.

In order to have information on the plasma dynamics beyond the 100 eV limit, series of time-gated spatial-spectral images were recorded upon ablation with the two laser wavelengths. In the plasma produced at 193 nm, intense lines related to Al, Al^+, Al^{++}, O, and O^+ could be identified. In contrast, only lines related to neutrals, i.e., Al and O, could be detected in the plasma produced at 248 nm. The maximum studied fluences were 2 J/cm^2 and 2.8 J/cm^2 upon ablation at 193 nm and 248 nm, respectively. Figure 3 shows

Reuse of AIP Publishing content is subject to the terms at: https://publishing.aip.org/authors/rights-and-permissions. Download to IP: 161.111.22.69 On: Fri, 08 Jul 2016 09:42:42

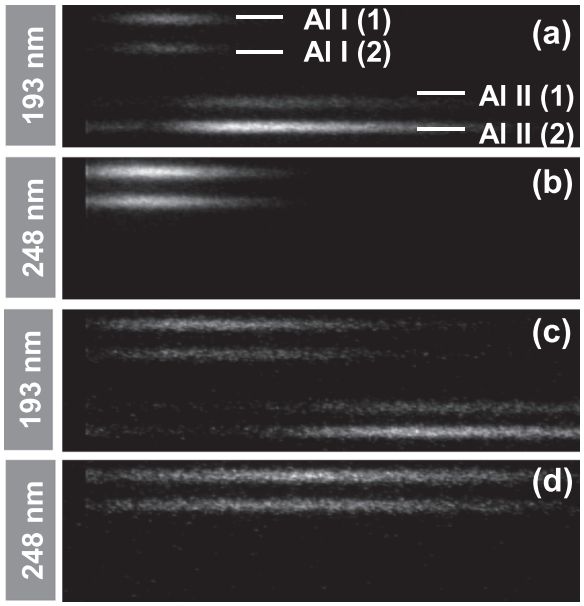

FIG. 3. Spectral (vertical)–spatial (horizontal) images acquired at 173 ns ((a) and (b)) and 453.5 ns ((c) and (d)) after the laser pulse and produced upon ablation at ((a) and (c)) 193 nm at 2 J/cm^2 and ((b) and (d)) 248 nm at 2.8 J/cm^2. The spectral range from top to bottom is 267-263 nm and the spatial interval is 1.15 mm. The neutral Al I lines are (1) 266.03 nm and (2) 265.24 nm and the ion Al II lines are (1) 263.50 nm and (2) 263.15 nm.

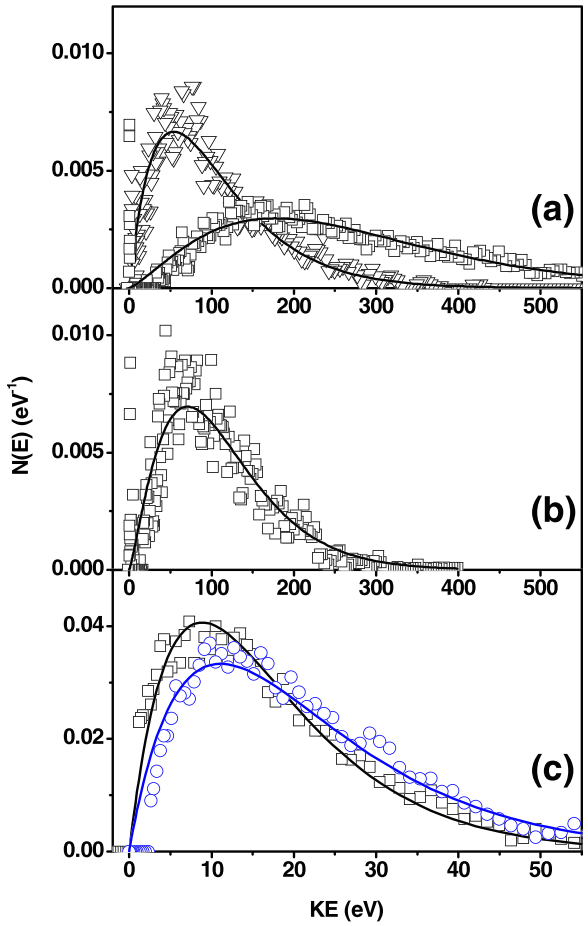

FIG. 4. KE distributions obtained from the spectral-spatial images acquired at 173 ns for (a) Al^+ (▽, 263.15 nm line) and Al^{++} (□, 569.6 nm line), (b) O^+ (388.21 nm line), and (c) Al (266.03 nm line) upon ablation at 193 nm at 2 J/cm^2 ((a) and (b)), (□) in (c) and 248 nm at 2.8 J/cm^2 ((○) in (c)). Full lines correspond to the best fit to the experimental data using a flux weighted shifted Maxwell-Boltzmann distribution.

spatial (horizontal)-spectral (vertical) images of the plasma obtained at two time delays with respect to the laser pulse and for the two laser wavelengths used for ablation. We have selected the spectral range of 263 to 267 nm where spectral lines of both Al^+ and Al can directly be compared and it becomes evident that the former are only seen for ablation at 193 nm. The images clearly show that the ions are much faster than the neutrals and neutrals are slightly faster upon ablation at 248 nm than at 193 nm.

The intensity profiles $I(z)$ of the excited emission transients along the expansion direction are converted into KE distributions using the method described elsewhere.[7] The spatial distribution profiles are first converted into velocity distributions $\Phi(v)$ by dividing the expansion axis units (z) by the corresponding delay time t at which the image was recorded and normalizing to unit area. The velocity distributions obtained are finally converted into KE distributions $N(E) = \Phi(v)|J(E)|$, using the relationship $E = 0.5\ mv^2$, where m is the mass of the specie and $J(E) = 1/mv$ the Jacobian.[7,29] This is done for $t > 100$ ns and $z > 2$ mm for which the continuum emission from *Bremsstrahlung* becomes negligible.

Figures 4(a) and 4(b) show as examples, the KE distributions of Al^{++}, Al^+ and O^+ obtained upon ablation at 193 nm for a time delay of 173 ns and a fluence of 2 J/cm^2 for which the relative amount of O^+, as measured with mass spectrometry, was already saturated (see Fig. 2(c)). In all cases, the distributions exhibit a maximum for KE < 100 eV that is followed by a long tail that expands well beyond 100 eV. Actually more than 44% of Al^+ have KE > 100 eV. Figure 4(c) shows the KE distributions of Al neutrals achieved by ablation at the two studied wavelengths. The range of KE over which the distribution extends is 10 times smaller than in the case of ions, in spite of the similar shape of the KE distributions generated by 193 nm ablation. The maximum appears around 10 eV and the tails become negligible around 60 eV. The main difference between the distributions obtained with the two ablation wavelengths is that the tail expands slightly to higher KEs when ablating at 248 nm.

It has usually been reported that the plasma expansion upon laser ablation is well described by a Maxwell-Boltzmann distribution.[1,20,23,24] We have fitted the optically obtained KE distributions (such as those shown in Fig. 4) with a flux-weighted shifted Maxwell-Boltzmann distribution[21,23,24,29]

$$I(v) \alpha v^3 \exp(-m(v - v_s)^2/2kT_{MB}),$$

where T_{MB} is the adjustable Maxwell-Boltzmann temperature of the distribution and v_s is the stream velocity that represent the speed of the ejected species. A good fit was achieved by considering $v_s = 0$ with the exception of Al^{++} and O^+ distributions upon ablation at 193 nm for which v_s was in the range 1–2 × 10^4 ms^{-1}. The fits of the experimental data shown in Fig. 4 are also included where it can be seen that the fittings are very good. From the fits, T_{MB} could

Reuse of AIP Publishing content is subject to the terms at: https://publishing.aip.org/authors/rights-and-permissions. Download to IP: 161.111.22.69 On: Fri, 08 Jul 2016 09:42:42

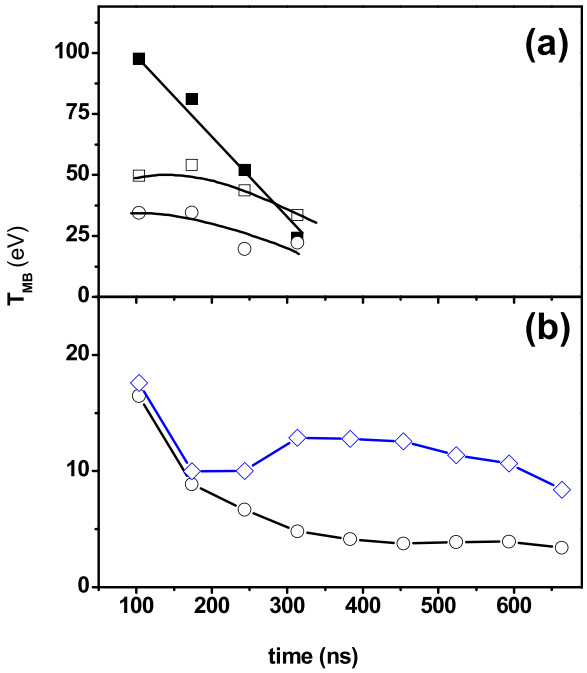

FIG. 5. Evolution of the Maxwell-Boltzmann temperature T_{MB} with time of (a) Al^{++} (■), Al^{+} (□), and O^{+} (○) upon ablation at 193 nm and (b) Al upon ablation at 193 nm (○) and 248 nm (◇). The fluences used are 2 J/cm^2 and 2.8 J/cm^2 for ablation at 193 nm and 248 nm, respectively, and we used the same spectral lines than those used for Fig. 4. Lines are guidelines.

be extracted and the results are plotted in Fig. 5. As expected, the higher temperatures are obtained for ions, that correspond from high to low to Al $^{++}$, Al^{+}, and O^{+} (Fig. 5(a)). A general decrease of temperature is observed as expected with increasing time and the steepest dependence corresponds to Al^{++}. Figure 5(b) shows the evolution of T_{MB} of Al neutrals at the two studied wavelengths where it can be seen that, even at short times (100 ns), the temperature of neutrals is less than half compared to the less energetic ions. The main difference of T_{MB} with the two ablation wavelengths is that it is almost constant (10–13 eV) for the case of 248 nm and times > 100 ns, while it decreases continuously with time when ablating at 193 nm.

The emitted line profile is the result of many broadening mechanisms and, for relatively low temperatures and high densities as it is the case for the laser ablated plasmas we are dealing with, it can be assumed to be dominated by collisions with electrons. This broadening is referred to as Stark broadening and becomes a well-established method for the estimation of electron densities (*Ne*).[25,30,31] The experimentally measured spectral lines were first fitted by Lorentzian functions. The Stark width is then obtained by deconvoluting the Gaussian widths (Doppler and instrumental).[32] In order to increase the precision, only results related to lines with Stark broadening higher than Gaussian have been used. *Ne* is finally determined from the database of Al Stark parameters assuming a linear dependence between *Ne* and the Stark width.[33,34] The shift of the peak position of the Lorentzian lines is related to the Stark shift and provides another means for determining *Ne* that has the advantage of being independent of line self-absorption. We have applied both methods to determine the space–time evolution of N_e from the 394.40 nm line of Al and achieved similar results. This agreement was similar to that reported elsewhere using the same line[35] thus confirming that self-absorption for this line can be neglected. From now on, results obtained using the Stark width method will be presented.

Assuming that the populations of the species in different excitation energy levels follow a Boltzmann distribution, the electronic temperature, T_e, can be determined using the Boltzmann-plot technique that relates the intensity of lines derived from transitions between energy levels of the same element.[25,31] We have considered 6 different lines for Al (256.79, 257.50, 265.24, 266.03, 394.40, and 396.15 nm) with upper energy levels from 3.14 to 4.8 eV. The intensity of the lines was corrected by the transmittance of the spectrometer and the Boltzmann-plot followed a linear behavior upon ablation at both studied wavelengths. The use of the Boltzmann-plot method requires that the plasma is optically thin[31] and thus self-absorption was carefully checked through the following three comparisons: the strength of lines within the same multiplet, the full width half maximum (FWHM) of lines in the same multiplet and the electron density (*Ne*) obtained from the Stark widths and shifts. We found no evidences for self-absorption in the Al lines used at times longer than 100 ns and for distances longer than 2 mm for which inverse *Bremsstrahlung* can be discarded.

Figures 6 and 7 show space-time plots of N_e and T_e upon ablation at 193 nm (a) and 248 nm (b), respectively. The plots have been built with 56 data (9 × 6) and a shading interpolation was performed in order to smooth the transition between neighboring data. Upon ablation at 248 nm, N_e and *Te* show a similar and expected behavior, i.e., the maximum intensity occurs for short times and distances. Instead, upon ablation at 193 nm, the maximum intensity of *Te* is achieved for long space and time values while the maximum intensity of *Ne* appears along the diagonal of the space-time plot, the intensity being slightly higher for short space and time values.

Space-time evolutions of *Ne* and *Te* could also be determined from ionic species for the case of ablation at 193 nm. For *Ne*, we have used the spectral line 281.61 nm of Al^{+}. The lines of O^{+} could not be used because they were too narrow. Figure 8(a) shows the results were it is seen that its features are similar to those of *Ne* determined from Al (Fig. 6(a)) in the sense that the maximum intensity occurs along the diagonal of the space-time plot. For *Te*, we tried to apply both the Boltzmann-plot technique used so far as well as the Saha-Boltzmann temperature using Al^{+} and Al lines but the results had no physical meaning. Therefore, we used O^{+} lines (464.91, 464.18, 459.09, 407.58, and 408.92 nm) with upper levels from 25.66 to 28.7 eV. Figure 8(b) shows the temporal and spatial evolution of T_e where it can be seen that it is significantly different than the *Te* determined from neutrals (Fig. 7(a)), while it is somehow similar to the N_e determined from ions (Fig. 8(a)).

IV. DISCUSSION

The results presented here evidence that the ionic composition, excitation, and kinetics of the plasma produced by

Reuse of AIP Publishing content is subject to the terms at: https://publishing.aip.org/authors/rights-and-permissions. Download to IP: 161.111.22.69 On: Fri, 08 Jul 2016 09:42:42

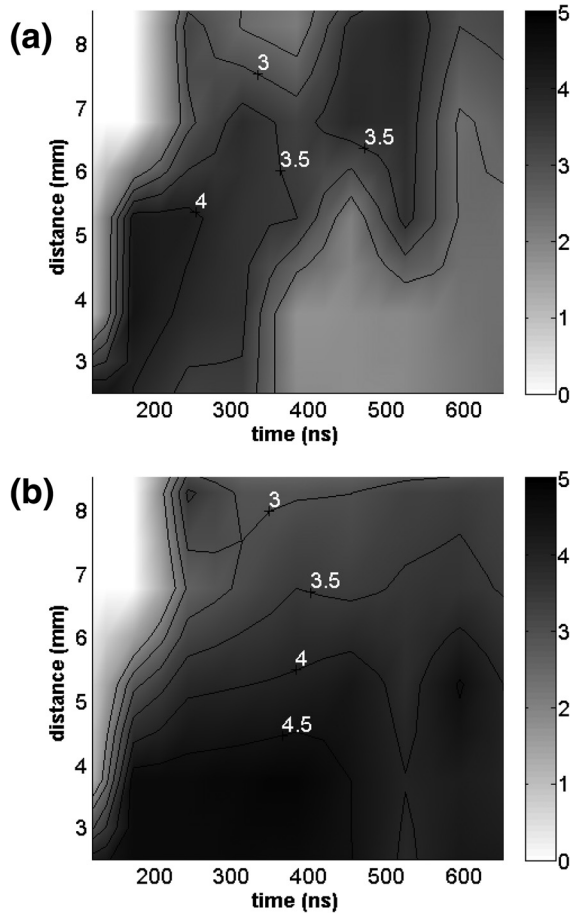

FIG. 6. Space-time plot of *Ne* obtained using the Stark width method and the Al lines upon ablation at (a) 193 nm at 2 J/cm^2 and (b) 248 nm at 2.8 J/cm^2. Lines of constant *Ne* have been plotted as guidelines and values are in 10^{17} cm^{-3} units.

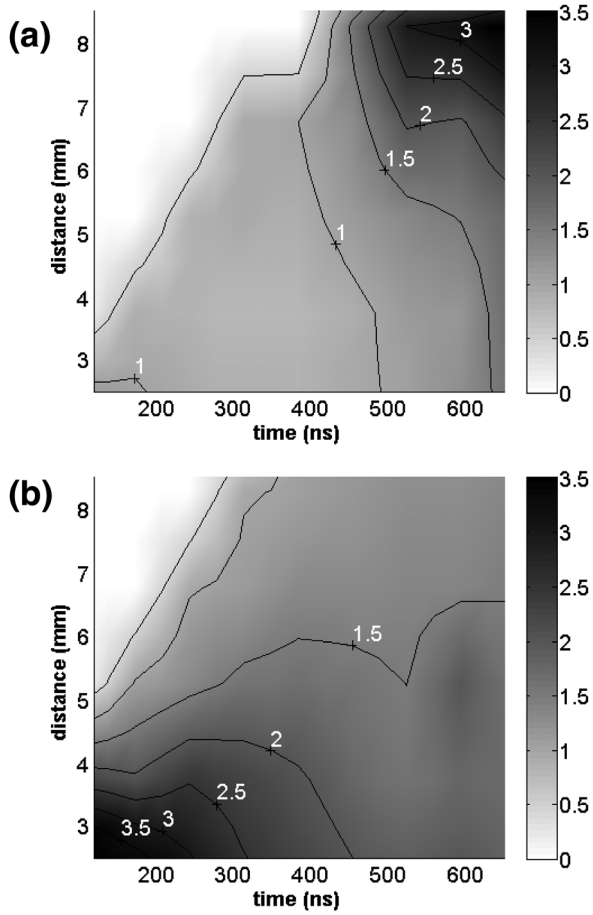

FIG. 7. Space-time plot of T_e obtained using the Boltzmann plot method and Al lines upon ablation at (a) 193 nm at 2 J/cm^2 and (b) 248 nm at 2.8 J/cm^2. Lines of constant *Te* have been plotted as guidelines and values are in eV.

laser ablation of ceramic Al_2O_3 at 193 nm and 248 nm are quite different. Furthermore, the degree of ion excitation at the latter wavelength is negligible at the fluences studied in this work. The photon energy of 6.4 eV when ablating at 193 nm is higher than the ionization potential of Al (5.98 eV) and it is thus enough to excite the $3p^2\ ^2S_{1/2}$ level of Al and to produce a high concentration of Al^+ through the loss of the outer electron. It has recently been reported that the fact that the plasma produced upon ablation of both Al_2O_3 and Al is dominated by energetic ions (with KEs up to 1 keV) is related to the existence of these direct or single-photon photoionization processes.[17] The 5.0 eV photons of 248 nm ablation have an energy lower than the ionization potential of Al but the energy is sufficient to photoionize many metal vapors via two or three steps involving low-energy intermediate excited states.[36] For the case of Al, this photon energy is higher than the energy required for photoionization from the first excited state of Al (3.14 eV) that was reported to be the reason for the differences observed upon ablation of Al with visible (2.31 eV) and UV (3.46 eV) photons.[23] Particularly, it was reported that the threshold for both observing ionized species and their saturation shift to smaller fluences when decreasing the wavelength, while the mean KEs were similar.[23] However, the special features associated to these indirect photoionization processes were noticeable for fluences $\approx$10 J/cm^2, i.e., much higher than those used in the present work.

Ions are the most energetic species, as detected both by mass spectrometry (ions with KE $<$ 100 eV in our case) and optical emission (only excited ions), upon ablation at 193 nm. The amount of O^+ increases with increasing fluence and becomes saturated for fluences around 1.5 J/cm^2 (Fig. 2) while the amount of Al^+ detected with optical emission is constant in the studied fluence range. In addition, the absolute amount of Al^+ is higher than that of O^+ (not shown) as reported earlier.[16] The KE distributions obtained from optical emission spectroscopy (Figs. 4(a) and 4(b)) show that there are ions of both types in the excited state with KE much higher than 100 eV and that the amount of excited Al^+ and O^+ with KE higher than 200 eV are, respectively, 12% and 8%. The comparison of these results with the KE distribution of Al^{++} (Fig. 4(a)) shows that they are the fastest ions, which allows the conclusion that Al ions are the fastest species in the plasma produced by ablation of Al_2O_3 at 193 nm. This conclusion is consistent with the similarities reported earlier between the plasmas produced by ablation of Al_2O_3 and Al targets at 193 nm and supports further the earlier conclusion based on Langmuir probe data that the ions having KEs up to 1 keV were mainly aluminum ions.[17]

Reuse of AIP Publishing content is subject to the terms at: https://publishing.aip.org/authors/rights-and-permissions. Download to IP: 161.111.22.69 On: Fri, 08 Jul 2016 09:42:42

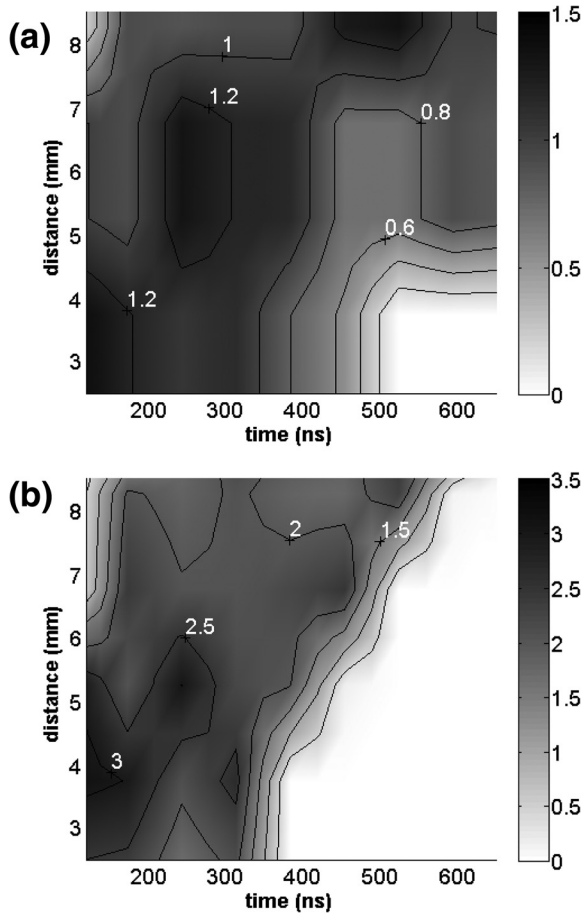

FIG. 8. Space-time plot of (a) *Ne* obtained using the Stark width method and the Al^+ lines and (b) T_e obtained using the Boltzmann plot method and O^+ lines, both upon ablation at 193 nm at 2 J/cm^2. Lines of constant *Ne* and *Te* have been plotted as guidelines and values are, respectively, in 10^{17} cm^{-3} and eV units.

The higher ionic content and excitation degree when ablating at 193 nm implies that there are much faster species in the plasma produced at this wavelength than at 248 nm. This becomes also evident from the Maxwell-Boltzmann temperatures plotted in Fig. 5(a) and obtained from the KE distributions of all species produced at 193 nm that are in the range 18–100 eV for times shorter than 200 ns. These values are much higher than the few eV reported earlier upon ablation of a Al_2O_3 and Al targets at longer wavelengths (355 nm and 532 nm) for fluences similar to the ones used in this work.[11,23]

The ion temperatures in Fig. 5 decrease as time increases as expected. However, the N_e and T_e space-time plots in Fig. 8 and obtained, respectively, from Al^+ and O^+ upon ablation at 193 nm do not follow the same evolution, i.e., the maximum values occur along the diagonal of these plots rather than at the origin. It is particularly noticeable that the high N_e in Fig. 8(a) ($>10^{17}$ cm^{-3} as obtained from Al^+) and the high T_e in Fig. 7(a) (3 eV as obtained from Al) are detectable for long times (500–600 ns) and long distances ($\approx$8 mm). Since the KE of ions upon ablation at 193 nm can be $>$1 keV,[17] the increase of temperature of Al after hundreds of ns must be related to neutralization of Al^+ ions that in the absence of a background gas, can only be due to recombination of Al^+ and electrons and thus, *Ne* and *Te* determine the probability of the process. This reasoning is in agreement with the absorption of the photons at 193 nm by the plasma and the production of single photon or direct photoionization of Al. Therefore, instead of a single population with a single temperature, two populations formed each by thermal (cold) and hot ions/electrons can briefly coexist in the corona region resulting in charge separation that can be sufficiently strong for accelerating the positive ions.[8,36] The KE distribution of Al^{++} in Fig. 3(a) that is shifted to higher values and the fact that the amount of these double charged ions does not saturate[16] provides further support to this reasoning. The repulsive forces that arise between the hot and cold populations can explain the need for a stream velocity necessary to fit the experimental KE distributions in Fig. 4 for Al^{++} and O^+ thus suggesting that the population of the latter is related to that of fast Al ions. This conclusion is consistent with the T_e plot in Fig. 8(b) obtained from O^+.

The recombination of hot electrons with Al^+ ions increases the population of Al that can interact with the hot cloud of electrons related to Al^+ ions. This becomes evident in Fig. 6(a) where one can distinguish two different contributions to N_e when ablating at 193 nm: one related to cold Al most likely associated to species directly ejected from the target and having temperatures $<$1 eV (Fig. 7(a)), and a hotter population (3–4 eV, Fig. 7(a)) related to neutralization of Al^+ at the front of the plasma. These two population scheme is also consistent with the results shown in Fig. 1(c) and the inset in Fig. 2(b), obtained by mass spectroscopy, which shows that there are two populations of neutrals, the hottest with KE $>$ 70 eV which increases with increasing fluence. At this point, it is noteworthy that the KE distribution of Al excited species show negligible species with KE $>$ 50 eV (Fig. 4(c)), while the KE distribution of all Al neutral species extend up to 100 eV and their amount is saturated (Figs. 1(c) and 2(b)). This allows us to conclude that at both studied wavelengths, there are Al neutrals in ground state that are faster than the excited ones. Upon ablation at 193 nm, the similarity between the KE distribution of the slow population (Fig. 1(c)) to that of excited neutrals (Fig. 4(c)) suggests that the former is associated to excited Al and therefore the fast Al neutrals formed by recombination of Al^+ must be in the ground state. Upon ablation at 248 nm, this comparison leads to the conclusion that the peak observed in Fig. 1(c) for KE $<$ 10 eV corresponds to excited neutrals, while the long tail up to 100 eV corresponds to the ground state neutrals.

Saturations effects by plasma shielding have been found in different laser induced plasmas and are more often encountered using longer wavelengths and higher fluences.[22,23] Our results show that they appear at fluences close to $\leq$1.5 J/cm^2 upon ablation at 193 nm. The high KEs of Al^+ allows them to travel at the front of the plasma and, because they absorb efficiently the laser photons, the slower species are shielded and therefore become little affected by an increase of the laser fluence. Similarly, if it is assumed that Al^{++} is produced by ionization of Al^+, it is not shielded and thus its amount must increase with fluence as reported earlier.[16] These results are consistent with those reported

Reuse of AIP Publishing content is subject to the terms at: https://publishing.aip.org/authors/rights-and-permissions. Download to IP: 161.111.22.69 On: Fri, 08 Jul 2016 09:42:42

elsewhere for ablation of Al targets at lower photon energies (355 and 532 nm)[22,23] for which photoionization can only occur through multiphoton processes. This requires much higher fluences that is consistent with the reported higher threshold for both saturation effects (>10 J/cm^2) and detecting Al^{++} (7–9 J/cm^2).[22] These reasoning is further supported by the results presented in Fig. 2(c) showing that O^+ becomes saturated for fluences around 1.5 J/cm^2 upon ablation at 193 nm, while there are no clear evidences of saturation for fluences up to 4 J/cm^2 upon ablation at 248 nm.

For the case of ablation upon 248 nm, the decrease of N_e (Fig. 6(b)) and T_e (Fig. 7(b)) with space and time is very similar to that reported in the literature upon ablation of ceramic Al_2O_3 at the same wavelength,[14] i.e., for a time around 100 ns, *Ne* is $\approx 6 \times 10^{17}$ cm^{-3} in the neighborhood of the target and becomes negligible for $z \approx 2.5$ mm from the target surface. The limited space-time window and number of points analyzed in the present work prevents us to determine the precise dependence of *Ne* and *Te* on *z*, but our results appear consistent with the z^{-n} dependence, where n is a number between 1 and 2, or the t^{-2} reported elsewhere for the case of ablation of Al targets at same[19] and longer wavelengths.[25] Therefore, we could conclude that the expansion of the plasma produced by ablation of Al_2O_3 at 248 nm is dominated by a single population and thus consistent with an adiabatic expansion.

The obtained results help to understand earlier reports on film properties and eventually to decide the appropriate wavelength for tailoring film properties, although this work has been focused to the study of the plasma produced by ablation of Al_2O_3 and no films were deposited. The special features of the plasma produced at 193 nm makes this wavelength essential for taking advantage of ion bombardment during growth such as sputtering, implantation or self-assembling processes.[2,5] In addition, energetic ion bombardment promotes the production of high density films.[3,5,10] In this respect, it is interesting to note that for achieving a refractive index higher than 1.65 by ablation at 248 nm, a fluence higher than 3.5 J/cm^2 was required,[3] while a value of 1.67 could be achieved by ablation at 193 nm with only 1.8 J/cm^2.[10] Besides, ion bombardment promotes amorphization,[5,10] while polycrystalline material could only be produced for low fluences at 1064 nm for which the KE of ions was kept low enough.[4]

V. CONCLUSIONS

Single-photon or direct photoionization of Al species upon ablation at 193 nm (i.e., with photon energies higher than the ionization potential of Al) leads to a dense and hot plasma dominated by Al^+ even for distances to the target up to 10 mm and times after the laser pulse longer than 500 ns. The coexistence of both hot/fast and thermal/slow populations of positive ions produces a repulsion of positively charged species and can accelerate the faster ions. The existence of these two populations has two important consequences. On the one hand, the hot electrons at the forefront of the plasma, related to the fast ions, promote recombination of Al^+ that leads to a second population of Al that is faster than the one produced by direct ejection from the target. On the other hand, the hot /fast population of Al species absorbs efficiently the photon energy and shields the slower part of the plasma leading to saturation effects at low fluences. The results achieved upon ablation at 248 nm for comparable fluences support further that the existence of these two populations upon ablation at 193 nm is directly related to single-photoionization processes of Al because *Ne* and *Te* decrease as space or time increases, and thus are dominated by the expansion of a single population. Furthermore, the amount of ions for 248 nm ablation is much smaller than that at 193 nm and the degree of ion excitation is negligible.

ACKNOWLEDGMENTS

This work has been partially supported by project IZK0Z2 of the Swiss National Science Foundation. R.P. acknowledges a grant from the JAE-doc program, co-funded by European Social Fund.

[1]D. B. Geohegan, *Pulsed Laser Deposition of Thin Films*, edited by D. B. Chrisey, and G. K. Hubler (John Wiley & Sons, Inc., 1994), Chap. V.
[2]J. Gonzalo, A. Perea, D. Babonneau, C. N. Afonso, N. Beer, J.-P. Barnes, A. K. Petford-Long, D. E. Hole, and P. D. Townsend, Phys. Rev. B **71**, 125420 (2005).
[3]J. Gottmann, G. Schlaghecken, and E. W. Kreutz, Appl. Phys. A **69**, S597–S600 (1999).
[4]L. Escobar-Alarcon, A. Arieta, E. Camps, S. Romero, M. Fernandez, and E. Haro-Poniatowski, Appl. Phys. A **93**, 605–609 (2008).
[5]A. Castelo, C. N. Afonso, E. Pesce, and E. Piscopiello, Nanotechnology **23**, 105603 (2012).
[6]V. Resta, J. Gonzalo, C. N. Afonso, E. Piscopiello, and J. García López, J. Appl. Phys. **109**, 094302 (2011).
[7]A. Perea, J. Gonzalo, C. Budtz-Jorgensen, G. Epurescu, J. Siegel, C. N. Afonso, and J. Garcia-Lopez, J. Appl. Phys. **104**, 084912-6 (2008).
[8]F. Claeyssens, S. J. Henley, and M. N. R. Ashfold, J. Appl. Phys. **94**, 2203–2211 (2003).
[9]L. Torrisi, F. Caridi, A. Picciotto, D. Margarone, and A. Borrielli, J. Appl. Phys. **100**, 093306 (2006).
[10]A. Suarez-Garcia, J. Gonzalo, and C. N. Afonso, Appl. Phys. A **77**, 779–783 (2003).
[11]F. Caridi, L. Torrisi, A. M. Mezzasalma, G. Mondio, and A. Borrielli, Eur. Phys. J. D **54**, 467–472 (2009).
[12]R. W. Dreyfus, R. Nelly, and R. E. Walkup, Appl. Phys. Lett. **49**, 1478–1480 (1986).
[13]J. E. Rothenberg and G. Koren, Appl. Phys. Lett. **44**, 664–666 (1984).
[14]R. M. Gilgenbach, C. H. Ching, J. S. Lash, and R. A. Lindley, Phys. Plasmas **1**, 1619 (1994).
[15]C. Ursu, O. G. Pompilian, S. Gurlui, P. Nica, M. Agop, M. Dudeck, and C. Focsa, Appl. Phys. A **101**, 153–159 (2010).
[16]R. J. Pelaez, C. N. Afonso, J. Chen, M. Esposito, T. Lippert, D. Stender, and A. Wokaun, J. Phys. D **45**, 285402 (2012).
[17]G. Baraldi, A. Perea, and C. N. Afonso, Appl. Phys. A **105**, 75–79 (2011).
[18]H. Wang and A. Salzberg, Appl. Phys. Lett. **59**, 935–937 (1991).
[19]E. Pérez-Tijerina, J. Bohigas, and R. Machorro, Rev. Mex. de Fís. **51**, 153–156 (2005).
[20]D. Bleiner, A. Bogaerts, F. Belloni, and V. Nassisi, J. Appl. Phys. **101**, 083301 (2007).
[21]F. Fuso, L. N. Vyacheslavov, G. Lorenzi, M. Allegrini, and E. Arimondo, Appl. Surf. Sci. **96–98**, 181–185 (1996).
[22]S. Amoruso, V. Berardi, R. Bruzzese, R. Velotta, N. Spinelli, and X. Wang, Appl. Surf. Sci. **138–139**, 250–255 (1999).
[23]S. Amoruso, M. Armenante, V. Berardi, R. Bruzzese, and N. Spinelli, Appl. Phys. A **65**, 265–271 (1997).
[24]R. S. Sage, U. B. Cappel, M. N. R. Ashfold, and N. R. Walker, J. Appl. Phys. **103**, 093301 (2008).
[25]P. Yeates and E. T. Kennedy, J. Appl. Phys. **108**, 093306 (2010).

Reuse of AIP Publishing content is subject to the terms at: https://publishing.aip.org/authors/rights-and-permissions. Download to IP: 161.111.22.69 On: Fri, 08 Jul 2016 09:42:42

[26]J. Kielkopf, J. Opt. Soc. Am. B **8**, 212 (1991).
[27]M. Bator, Y. Hu, M. Esposito, C. W. Schneider, T. Lippert, and A. Wokaun, Appl. Surf. Sci. **258**, 9355–9358 (2012).
[28]J. Siegel, G. Epurescu, A. Perea, F. J. Gordillo-Vazquez, J. Gonzalo, and C. N. Afonso, Opt. Lett. **29**, 2228–2230 (2004).
[29]F. M. Zimmermann and W. Ho, Surf. Sci. Rep. **22**, 127–247 (1995).
[30]N. Konjević, M. Ivković, and S. Jovićević, Spectrochim. Acta, Part B **65**, 593–602 (2010).
[31]J. Aguilera and C. Aragón, Spectrochim. Acta, Part B **59**, 1861–1876 (2004).
[32]J. T. Davies and J. M. Vaughan, Astrophys. J **137**, 1302 (1963).
[33]N. Konjević and W. L. Wiese, J. Phys. Chem. Ref. Data **19**, 1307 (1990).
[34]N. Konjević, A. Lessge, J. R. Fuhr, and W. L. Wiese, J. Phys. Chem. Ref. Data **31**, 819 (2002).
[35]C. G. Parigger, J. O. Hornkohl, and L. Nemes, Appl. Opt. **46**, 4026–4031 (2007).
[36]C. R. Phipps and R. W. Dreyfus, in *Laser Ionization Mass Analysis*, edited by A. Vertes, R. Gijbels, and F. Adams (Wiley, New York, 1993), p. 369.

Reuse of AIP Publishing content is subject to the terms at: https://publishing.aip.org/authors/rights-and-permissions. Download to IP: 161.111.22.69 On: Fri, 08 Jul 2016 09:42:42